Title

Estimation of air-sea CO_2 fluxes in the Bay of Biscay based on empirical relationships and remotely sensed observations.

Authors

Padin, X.A.[1], Navarro, G. [2], Gilcoto, M.[1], Rios, A.F.[1] and Pérez, F.F.[1]

[1] Instituto de Investigacións Mariñas (CSIC). Eduardo Cabello 6, 36208 Vigo, Spain

[2] Instituto de Ciencias Marinas de Andalucía (CSIC). Avda. República Saharaui, s/n, 11510, Puerto Real (Cadiz), Spain

Corresponding author

Padin, X.A.

Instituto de Investigacións Mariñas (CSIC). Eduardo Cabello 6, 36208 Vigo, Spain

Telf. +34-986-231930 (Ext. 377)

Fax. +34-986-292762

E-mail: padin@iim.csic.es

Keywords

Bay of Biscay, carbon dioxide; air-sea flux; AVHRR; SeaWiFS

Abstract

An empirical algorithm has been developed to compute the sea surface CO_2 fugacity (fCO_2^{sw}) in the Bay of Biscay from remotely sensed sea surface temperature (SST_{RS}) and chlorophyll *a* (chl a_{RS}) retrieved from AVHRR and SeaWiFS sensors, respectively. Underway fCO_2^{sw} measurements recorded during 2003 were correlated with SST_{RS} and chl a_{RS} data yielding a regression error of 0.1±7.5 μatm (*mean*±*standard deviation*). The spatial and temporal variability of air-sea fCO_2 gradient (ΔfCO_2) and air-sea CO_2 flux (FCO_2) was analyzed using remotely sensed images from September 1997 to December 2004. An average FCO_2 of -1.9±0.1 $mol \cdot m^{-2} \cdot yr^{-1}$ characterized the Bay of Biscay as a CO_2 sink that is suffering a significant long-term decrease of 0.08±0.05 $mol \cdot m^{-2} \cdot yr^{-2}$ in its capacity to store atmospheric CO_2. The main parameter controlling the long-term variability of the CO_2 uptake from the atmosphere was the long-term changes of the air-sea CO_2 transfer velocity (57%) followed by the SST_{RS} (10%) and chl a_{RS} (2%).

1. Introduction

Oceans play a decisive role in mitigating the effects of climate change storing huge amount of the CO_2 released to the atmosphere (Sabine et al., 2004). The CO_2 cycle in the oceans is mainly controlled by the ocean circulation and the biological activity (i.e. photosynthesis and remineralization) in the water, mainly in the upper layer (Sarmiento and Le Queré, 1996). The capacity of the oceans to absorb the excess of CO_2 from the atmosphere is a key parameter to predict future atmospheric CO_2 levels and to estimate the oceanic uptake of anthropogenic CO_2. However, the quantification of the CO_2 uptake and its storage has large uncertainties derived from the difficulty of discriminating the natural from the anthropogenic CO_2 signal (Schuster and Watson, 2007). Furthermore the existence of different parameterizations for the kinetic of CO_2 exchanges at the air-sea boundary and, most importantly, the sparse sampling of surface waters are important issues in the correct description of air-sea CO_2 fluxes (FCO_2).

In order to mitigate the scarcity of CO_2 observations, sampling networks have been developed from different observation platforms, such as, ships, drifter buoys and moorings that largely increased the *in situ* CO_2 measurements over the last years. Several international projects (JGOFS, GLODAP, WOCE, CARINA) have coordinated most of the synthesis efforts resulting in inventories of CO_2 measurements with improved spatial and temporal resolution. This growing dataset of *in situ* CO_2 observations has appreciably enhanced and refined the FCO_2 estimations at different scales (Olsen et al., 2004; Lefevre et al., 2004; Nelson et al., 2001).

Along the same line, extrapolation techniques have been developed for minimizing the uncertainties caused by the extrapolation of observed CO_2 fugacity in seawater (fCO_2^{sw}). These fCO_2^{sw} empirical algorithms based on sea surface temperature (SST) have been frequently used in order to reproduce the strong temperature control on the fCO_2^{sw} variability due to thermodynamic processes, water mixing events and even biological production. For example, the fCO_2^{sw} distribution has been extrapolated to different geographical scales applying the empirical algorithms to climatological products or *in situ* measurements (Lefevre and Taylor, 2002; Tans et al., 1990; Metzl et al., 1995).

The application scope of these extrapolation techniques has been extended with the inclusion of remotely sensed variables as inputs providing a synoptic view at near real time. Thus, maps of fCO_2^{sw} fields were firstly built from remotely sensed SST (SST_{RS}) (Stephens et al., 1995; Goyet et al., 1998; Lee et al., 1998; Hood et al., 1999; Nelson et al., 2001; Olsen et al., 2004). Subsequently, the inclusion of chl *a* retrieved from satellite observations (chl a_{RS}), as an additional proxy of the biological CO_2 uptake significantly improved the fCO_2^{sw} extrapolation (Ono et al., 2004).

The ECO project was planned and developed to increase the number of fCO_2^{sw} observations in the Bay of Biscay using ships of opportunity. Being part of the most important sink of atmospheric CO_2 (Takahashi et al., 2002), the estimation of FCO_2 fluxes in this region is important for improving the estimation of the stored CO_2. The fCO_2^{sw} measurements recorded during repeated ECO cruises in 2003 were fitted to nonlinear equations using SST_{RS} and chl a_{RS} according to Ono et al. (2004). Moreover the long-term variability of fCO_2^{sw} was also analyzed assuming analogous relationships in the Bay of Biscay between September 1997 and December 2004.

2. Material and methods

2.1 Data and shipboard procedures

Continuous underway measurements in the Bay of Biscay were retrieved from ships of opportunity belonging to the Suardíaz Company float (*RO-RO L'Audace* and *RO-RO Surprise*). The route between Vigo (Spain) – St. Nazaire (France) shown in Figure 1 was repeatedly sampled during 2003, making a total of 64 tracks.

The seawater molar fraction of CO_2 (xCO_2^{sw}) was measured using an autonomous equipment designed by the Instituto de Investigaciones Mariñas (IIM-CSIC, Vigo), following Körtzinger et al. (1996). Surface seawater is drawn from the ship's cooling water tank where a pt100 temperature probe continuously recorded SST, with an accuracy of ±0.1ºC. The water was pumped from the cooling water tank to the autonomous equipment at a high flow rate in order to reduce any water warming along the pipe length, the temperature rise was kept <1ºC. At the autonomous equipment, the

continuous water flow passes through an equilibrator, which is vented to the atmosphere, and combines the bubble (Takahashi, 1961) and the laminar flow type (Poisson et al., 1993).

The molar fraction of CO_2 (xCO_2) was determined by a non-dispersive infrared gas analyser (Licor®, LI-6262) that has a minimum accuracy of ±0.3 ppm for the entire CO_2 range. At the beginning and the end of each transit (which takes 26 hours), the analytical equipment was calibrated with two gas standards: a CO_2-free air for the blank and a 375±0.1 ppmv CO_2 standard certified by Instituto Meteorológico Nacional de Izaña (Canary Islands). The seawater CO_2 fugacity (fCO_2^{sw}) was obtained from xCO_2^{sw} as described in DOE (1994), correcting for the temperature shift using the empirical equation proposed by Takahashi et al. (1993). In a parallel line to the equilibration unit, underway measurements of chl *a* (sensitivity 0.03 $\mu g \cdot L^{-1}$) were also performed with a fluorometer (WETLabs). The fluorometer measurements were calibrated with discrete chl *a* samples collected at 4 locations along the track every two cruises (Fig. 1). Subsequently, the data set, logged with a 1 minute frequency, was averaged every 5 minutes resulting in 8798 observations along the cruise track shown in Figure 1.

2.2 Remotely sensed SST and chl a data

Pathfinder v5 SST data are derived from the five-channel Advanced Very High Resolution Radiometers (AVHRR) on board NOAA-7, 9, 11, 14, 16 and 17 polar orbiting satellites. The basic product consists of a pair of daily, global SST_{RS} fields at a spatial resolution of 4 km, representing ascending (daytime) and descending (night time) orbits separately. The data used goes from September 1997 to December 2004. Pathfinder SST data are available via anonymous ftp from the Jet Propulsion Laboratory (JPL) web site (ftp://podaac.jpl.nasa.gov). Along with the Pathfinder SST data, quality flags can also be obtained. Clouds are identified from these quality flags so that each user can decide which mask should be applied to the data.

Daily Sea-viewing Wide Field-of-view Sensor (SeaWiFS) SMI (Standard Mapped Image) L3 (reprocessing 5.1, July 2005) chl *a* concentration data were retrieved from the NASA Goddard Space Flight Center (GSFC) Distributed Active Archive Center (DAAC) (ftp://oceans.gsfc.nasa.gov). SMI-L3 daily products are generated from GAC

(Global Average Coverage) data by binning data in time and space to give global coverage from cells of equal area, with a spatial resolution of 9 km (Campbell et al. 1995). SeaWiFS is described in Hooker et al. (1992) and up-to-date information can be found at http:// seawifs.gsfc.nasa.gov. SeaWiFS measures normalised water-leaving radiance at six bands on the visible spectrum (400-700 nm) that add up to convey a single measurement of "ocean colour". Various chl *a* algorithms have been developed to estimate the surface concentration of chl *a* from each ocean colour measurement (e.g., O'Reilly et al. 1998). Once again, the data used go from September 1997 to December 2004.

2.3 fCO_2^{sw} extrapolation algorithm

The *in situ* fCO_2^{sw} measurements gathered during ECO cruises were fitted with second-order multiple polynomials using SST_{RS} and chl a_{RS} observations as independent variables.

$$_{RS}fCO_2^{sw} = A \cdot SST_{RS} + B \cdot SST_{RS}^2 + C \cdot \text{chl } a_{RS} + D \cdot \text{chl } a_{RS}^2 + E \qquad (1)$$

The letters A to E are the fitting coefficients computed from a Marquard – Levengerg algorithm.

As described in Ono et al (2004), the algorithm (Eq. 1) was developed from the empirical relationships proposed by Lee et al. (2000), Millero et al. (1998) and Goes et al. (2000). The SST_{RS} and chl a_{RS} values were selected from pixels centred within ±2.8 km and ±6.3 km from the cruise track and from overpasses within ±6 h and ±12 h of the time of any fCO_2^{sw} measurement, respectively.

Latitude and longitude were also included in a preliminary fit as independent variables in an attempt to improve the algorithm proposed by Ono et al. (2004). Nevertheless, the geographical location of the fCO_2^{sw} measurements within the sampled region was not statistically significant due to the high homogeneity of biogeochemical properties of the Bay of Biscay.

Once the coefficients in the Eq. 1 have been determined, the empirical algorithm is spatially extrapolated to an area of ~10^7 km^2 between 44 – 46 ºN and 9 – 3 ºW for studying the spatial fCO_2^{sw} variability in the inner part of the Bay of Biscay (Fig. 1). The fCO_2^{sw} variability at long-term trend was also analyzed from the spatially and temporal extrapolation of the observed relationships from the first available images of SeaWiFS in September 1997 to December 2004. A year-to-year rise of ~1.7µatm·yr^{-1} corresponding to the long-term variability of the atmospheric fCO_2 (fCO_2^{atm}) was added to every fCO_2^{sw} computations (Olsen et al., 2003). This rate of fCO_2^{atm} change was estimated from atmospheric xCO_2 recordings in nearby meteorological stations belonging to the NOAA/ESRL Global Monitoring Division (Padin et al., 2007).

2.4 Estimation of air-sea CO_2 flux fields

The CO_2 exchange between the atmosphere and the ocean, (FCO_2, in mol·m^{-2}·yr^{-1}) was calculated using the following equation:

$$FCO_2 = \alpha \, k \, S \, \Delta fCO_2 \qquad (2)$$

Where k (cm h^{-1}), is the monthly mean CO_2 transfer velocity calculated using the Wanninkhof's coefficients (Wanninkhof, 1992) and monthly estimations of wind speed (WS) obtained from the NCEP/NCAR Reanalysis project (NOAA-CIRES Climate Diagnostics Center, http://www.cdc.noaa.gov/). The CO_2 solubility in seawater (S, mol·kg^{-1}·atm^{-1}) was calculated from Weiss (1974) using SST_{RS} and salinity from climatological atlas of the World Ocean Database 2001 (http://www.nodc.noaa.gov/). The parameter α is the unit conversion factor. The ΔfCO_2 is the air-sea fCO_2 difference, i.e. $fCO_2^{sw} - fCO_2^{atm}$, where fCO_2^{sw} was estimated as explained in section 2.3 and fCO_2^{atm} as follows. The monthly values of atmospheric molar fraction of CO_2 (xCO_2^{atm}) in the Bay of Biscay (45ºN) was linearly interpolated meridionally from xCO_2^{atm} observations recorded in the meteorological stations of Azores (38.77ºN) and Mace Head (53.55ºN). To convert the xCO_2^{atm} to fCO_2^{atm}, the water vapour pressure (pH_2O, in atm) was calculated from in situ temperature (T_{is}, in ºC) according to Cooper et al. (1998) and assuming a 0.3% decrease between pCO_2^{atm} and fCO_2^{atm} (Weiss 1974) to be sufficiently accurate.

$$pCO_2^{atm} = xCO_2^{atm} \cdot (p_{atm} - pH_2O) \quad (3)$$

$$pH_2O = 0.981 \cdot \exp(14.32602 - (5306.83/(273.15 + T_{is}))) \quad (4)$$

Gridded fields of daily mean sea level pressure (p_{atm}) were also provided from the NCEP/NCAR Reanalysis project. We used monthly NCEP/NCAR SLP fields on a 2.5x2.5 degree grid for the study area during the period 1997 – 2004.

3. Results and Discussion

3.1. Correlation of shipboard fCO_2^{sw} with remotely sensed SST and chl a

The agreement between the remotely sensed observations and the *in situ* measurements gathered during ECO cruises is shown in Figure 2. Similarly to Olsen et al. (2004), we found that neither temporal nor spatial distances correlated with the differences between SST and chl *a* recorded during 2003 and from satellite sensors. Therefore, no interpolation in the co-location procedure was necessary.

The SST_{RS} that correspond to the skin temperature showed an underestimation of -0.2±0.6 ºC (*mean±standard deviation*) in comparison to the *in situ* SST throughout the seasonal cycle. This is explained from the fact that the skin temperature is not exactly the same as the corresponding to the 3 meter depth measured by the continuous underway system (Kilpatrick et al., 2001; Robertson and Watson, 1993). The disagreements between chl a_{RS} and chl *a* also displayed a negative offset of -0.15±0.33 $mg \cdot m^{-3}$. The maximum differences of about 2 $mg \cdot m^{-3}$ were observed from March to June during the intense growth of the phytoplankton communities. Significant discrepancies of around 1 $mg \cdot m^{-3}$ were also found in October associated to a secondary bloom that usually followed the broken of summer stratification.

The number of collocated observations of SST_{RS} and chl a_{RS} only achieved 19 and 26%, respectively, of the 5-minutely averages of fCO_2^{sw} measurements. Thus, the coefficients for Eq. 1 were estimated from 874 data that represent about 10% of the average fCO_2^{sw} recordings.

$_{RS}fCO_2^{sw}$ = -23(±2)·SST_{RS} + 0.8(±0.05)·SST_{RS}^2 – 46(±3)·chl a_{RS} + 12(±1)·chl a_{RS}^2 + 508

The algorithm fitted the *in situ* fCO_2^{sw} measurements with a root mean square (rms) error of 0.1±7.5 μatm for the year 2003 (Figure 2c). This rms error is appreciably lower than ±14 and ±17 μatm reported by Ono et al. (2004) in large areas of subtropical and subpolar North Pacific Ocean, respectively. On the other hand, Olsen et al. (2004) obtained an error of ±9.5 μatm from measurements gathered in the Caribbean Sea using a different algorithm based on a linear relationship between SST_{RS} and fCO_2^{sw} including the geographical location. This algorithm was applied to our dataset and produced a worse fitting of *in situ* fCO_2^{sw} measurements in the Bay of Biscay with an average discrepancy of -2±13 μatm.

Other alternative algorithms were previously evaluated before choosing the best option to reproduce the observed fCO_2^{sw} variability as well. For instance, a quadratic factor of SST_{RS} including the location of measurement fitted the seasonal distribution of fCO_2^{sw} with a rms error of -2±10 μatm. Furthermore the selected algorithm was also re-evaluated studying the result obtained from remotely sensed variables with different frequency. Using weekly fields of SST_{RS} and chl a_{RS} instead 6-hourly and daily fields, respectively, the number of co-located fCO_2^{sw} measurements sensible increased up to 5102 although the error appreciably rose to -0.4±10.9 μatm. Thus, the empirical algorithm proposed by Ono et al. (2004) was chosen as the optimal fit explaining an 85% of the total fCO_2^{sw} variability during the ECO cruises. The relative contribution of each variable used in the fCO_2^{sw} prediction was determined from a fixed nonlinear regression model. So, SST_{RS} and chl a_{RS} that were statistically significant (p-value<0.05), they explained 71% and 14% of the observed fCO_2^{sw} variability, respectively.

Generally speaking the *in situ* fCO_2^{sw} observations in the Bay of Biscay were satisfactorily reproduced by the remotely sensed variables, especially from June to September (Fig. 2c). However, some notable differences between predicted and observed fCO_2^{sw} were found, especially, during wintertime and the late stage of the spring bloom. The *in situ* fCO_2^{sw} observations were underestimated by the algorithm as much as 15 μatm in January and March whereas an overestimation of more than 20 μatm during May yielded maximum disagreements. According to Figure 3, our

algorithm does not reproduce in situ fCO_2^{sw} values around 305 μatm for the chl a_{RS} range of 0.3 – 0.8 $mg \cdot m^{-3}$ yielding the mentioned overestimation. These fCO_2^{sw} measurements were recorded after the characteristic chl *a* maximum developed during the spring that disappeared due to sedimentation or grazing processes. As it was previously reported (Stephen et al., 1995; Ono et al., 2004), the late stage of the spring bloom is a critical period for fCO_2^{sw} prediction since the relative slow velocity of air-sea CO_2 equilibration preserves the fingerprint of the biological drawdown well beyond the chl *a* vanishing.

Another aspect to take into account in the analysis of these disagreements is the occurrence of coccolithophore blooms that were previously reported in the Bay of Biscay during the late spring (Beaufort and Heussner, 1999; Lampert et al., 2002; Harlay et al., 2006). The calcification produced during the coccolith growth, usually *Emiliania huxleyi*, reduces the alkalinity counteracting the photosynthetic CO_2 uptake and increasing the fCO_2^{sw}. Thus, surface waters during events of coccolithophore blooms behave as a small CO_2 source rather than a sink (Tyrrell and Taylor, 1995). As was described by Robertson et al. (1994), an intense development of coccolithoph assemblages in the North Atlantic could increase by 15 μatm the seasonal fCO_2^{sw} cycle blocking on average a 17% of the total CO_2 uptake and with blockin peaks reaching 35%.

The presence of *Emiliania huxleyi* blooms during ECO cruises was checked from remotely images of SeaWiFS sensor based on two algorithms to detect coccolithophorid blooms. As a first approximation, we used final products (http://cics.umd.edu/~chrisb/ehux_www.html) developed according to Brown and Yoder (1994) methodology that showed no bloom during 2003. Then, we processed images of SeaWiFS nLw_555 according to Raitsos et al. (2006) from 1997 to 2004 in order to estimate the coccolithophore abundance. These maps showed three vast blooms events in the inner part of the Bay of Biscay, especially during 2004. For that reason, an optimum algorithm should include the potential effect of coccolith production on the fCO_2^{sw} distribution in spite of being usually minor.

3.2. Climatological fCO_2^{sw} maps estimated from the empirical algorithm

The spatial variability of fCO_2^{sw} in the Bay of Biscay was studied from climatological fCO_2^{sw} maps built using SST_{RS} and chl a_{RS} maps for each month computed from images retrieved between January 1998 and December 2004 . The comparison between the monthly fCO_2^{sw} fields and the *in situ* fCO_2^{sw} measurements showed a disagreement of 2±12 μatm (n=8798) significantly higher than the 0.1±7.5 μatm obtained using the short-term maps of SST_{RS} and chl a_{RS}. Subsequently, monthly fields of ΔfCO_2 and FCO_2 were computed with a spatial resolution of 9 km^2 for the extrapolation region of the Bay of Biscay.

The four ecological seasons proposed by Longhurst (1998) in the region were graphically depicted in the Figure 4 from the climatological maps of January (winter), April (spring), July (summer) and October (autumn). The winter season is characterized by the homogenization of biogeochemical variables in the surface waters due to the intense mixing processes (Fig 4). So, the combination of SST_{RS} and chl a_{RS} yielded a homogeneous ΔfCO_2 field of -37±1 μatm during January. The notable growth of phytoplankton community during April turned the uniform ΔfCO_2 distribution of winter into the patchy pattern typically shown by chl *a* during the spring. The photosynthetic activity lead the air-sea fCO_2 disequilibrium in the Bay of Biscay to maximum values of around -60 μatm and showing an average ΔfCO_2 value of -56±4 μatm (Fig. 4). Contrary chl a_{RS} is almost negligible during summer due to full consumption of nutrients in the mixed layer becoming SST_{RS} into the key variable to explain the ΔfCO_2 distribution. The thermodynamic effect of summer warming on fCO_2^{sw} variability reduced the air-sea fCO_2 differences throughout the Bay of Biscay even causing a slight CO_2 oversaturation in relation to the atmosphere at the eastern boundary (Fig. 4). The temperature control is also evident from the east-west fCO_2^{sw} gradient that follows the known eastward warming of surface waters in the Bay of Biscay (Planque et al., 2003; Koutsikopoulos and Le Cann, 1996). So, the longitudinal variability during this season explains 79% (p-value<0.01) of the fCO_2^{sw} distribution showing a fCO_2^{sw} increase toward the inner part of 2.10±0.02 μatm·ºE. The onset of autumn meteorological conditions produces the increase of turbulent mixing and the deepening of the thermocline breaking the previous steady stratification of the upper layers. Therefore the autumn ΔfCO_2 distribution, which average value is -18.5±2.6 μatm, is roughly the intermediate image of the summer east-west gradient and the winter homogeneous pattern.

The climatological FCO_2 maps indicate that the Bay of Biscay generally behaves as a homogenous sink (Fig. 4). So, the rate of oceanic CO_2 uptake in our study region during winter is -4.0±0.1 mol·m^{-2}·yr^{-1}. That is very similar to -4.3±0.3 mol·m^{-2}·yr^{-1} the estimated flux during spring when ΔCO_2 values were significantly higher. This finding highlights the decisive kinetic control of WS over the air-sea CO_2 exchange since there were small differences found between winter (9.7±1.7 m·s^{-1}) and spring (8.3±1.4 m·s^{-1}) winds. The average FCO_2 during July was closer to equilibrium, namely, -0.4±0.2 mol·m^{-2}·yr^{-1} even acting as CO_2 source to the atmosphere in near shore regions. Finally during autumn, the Bay of Biscay increased the atmospheric CO_2 uptake to -1.4±0.2 mol·m^{-2}·yr^{-1} showing a distribution closer to the wintertime one.

3.3 Long-term fCO_2^{sw} variability in the Bay of Biscay

The long-term fCO_2^{sw} variability in the Bay of Biscay was estimated assuming that the obtained relationships are valid from September 1997 to December 2004. Long-term trends of every variable with the exception of chl a_{RS} were computed fitting the distribution of SST_{RS}, ΔfCO_2, WS and FCO_2 by means of the least squares method to a theoretical curve of combination of two components: the annual linear tendency and a seasonal cycle with four harmonics. Spatial means and standard deviations of the monthly maps of SST_{RS}, chl a_{RS}, WS with the monthly computations of ΔfCO_2 and FCO_2 are shown in Figure 5.

The ΔfCO_2 values (Fig. 5c) ranged from -61 to 26 μatm throughout the study period with an annual range of 52±11 μatm (Table 1). Maximum ΔfCO_2 values of 11±9 and 6±9 μatm were reached between August and September (Table 1), respectively, coinciding with the annual maximum of SST_{RS} (Table 1; Fig. 5a). Additionally minimum ΔfCO_2 values of -55±6 μatm were directly linked to the maximum phytoplankton growth of 0.83±0.24 mg·m^{-3} observed during April (Table 1; Fig. 5b). The effect of the photosynthetic activity is also clearly appreciable in the ΔfCO_2 decrease found during the successive autumn (Table 1; Fig. 5c) in response to the secondary phytoplankton bloom.

Even though no ΔfCO_2 variability was found at long-term trend, the homogeneous winter values of SST_{RS} and chl a_{RS} yielded a flat shape in the ΔfCO_2 values from December to February (Table 1) that clearly draws a winter-to-winter linear ΔfCO_2 increase from 1998 to 2004. Thus, the average ΔfCO_2 during the successive winters showed a significant long-term increase of 0.7 ± 0.2 $\mu atm \cdot yr^{-1}$ (p-value<0.05) (Fig. 6c). No other significant long-term ΔfCO_2 trend has been found for any of the other three seasons.

In relation to the SST_{RS} trend (Fig. 6a), the Bay of Biscay got cold throughout our study period with a year-to-year rate of -0.06 ± 0.02 $^{o}C \cdot yr^{-1}$ (p-value<0.05). It is worth underlining that the temperature effect on fCO_2^{sw} estimations changes seasonally and shows two different trends. According to the computed algorithm coefficients, the sign of the SST_{RS} - fCO_2^{sw} relationship changes at 14.4ºC since at this temperature the first partial derivative with respect to SST_{RS} is zero. Thus, SST_{RS} values larger than 14.4 ºC retrieved from May to November (Table 1) show a positive correlation corresponding to the thermodynamic effect of temperature on the fCO_2^{sw} variability. Contrary, a negative SST_{RS} - fCO_2^{sw} correlation dominated the colder months standing for the direct relationship between the cooling of surface waters and the fCO_2^{sw} rise due to entrainment of CO_2-rich subsurface waters by vertical mixing processes.

Due to poorly fitted of chl a_{RS} distribution (Fig. 5b) from the harmonics and a linear tendency, chl a_{RS} trend was assessed following Gregg et al. (2005). So, the seasonal cycle (averaging the time series for each month of the year) is subtracted of original chl a_{RS} values producing monthly anomalies that are annually averaged. The chl a_{RS} variability at long scale was assessed from the linear trend of these annual averages of monthly chl a_{RS} anomalies showing a decrease of -0.010 ± 0.002 $mg \cdot m^{-3} \cdot yr^{-1}$ (p-value<0.05). The declination of the photosynthetic activity observed in the Bay of Biscay agrees the chl a_{RS} reduction found in close oceanic waters during the period 1998 – 2003 (Gregg et al., 2005).

Contrary to the significant trends of SST_{RS} and chl a_{RS}, WS distribution did not show any significant long-term variability although clear interannual changes were really appreciated at seasonal scale (Fig. 6c).

The FCO_2 estimations derived from the ΔfCO_2 computations showed an average FCO_2 value throughout the study period of -2.5±0.3 $mol \cdot m^{-2} \cdot yr^{-1}$ (Fig. 5e), which means an annual uptake of 2.9 $TgC \cdot yr^{-1}$ in the extrapolation window. The annual FCO_2 averages spanned from -2.0 to -2.9 $mol \cdot m^{-2} \cdot yr^{-1}$ exceeding the average FCO_2 of -1.84 $mol \cdot m^{-2} \cdot yr^{-1}$ for European marginal seas between 32ºN and 57ºN reported by Borges et al. (2005). Thus, our estimates characterize the Bay of Biscay as a strong sink of atmospheric CO_2, mainly due to the important subduction of mode waters (Paillet and Mercier, 1997) present in the region. Nevertheless, the most outstanding finding in our study is the weakening of the capacity as atmospheric CO_2 sink of the Bay of Biscay at long-term trend of 0.08±0.05 $mol \cdot m^{-2} \cdot yr^{-2}$ (p-value<0.2). This reduction of the oceanic CO_2 uptake represents a net loss of 3% of mean value over the 7 years that is equivalent to 0.09 $TgC \cdot yr^{-1}$. Recent studies also pointed out the reduction of sink capacity of atmospheric CO_2 in the Eastern North Atlantic Ocean (Lefevre et al., 2004; Omar and Olsen, 2006; Corbiere et al., 2006; Schuster and Watson, 2007; Patra et al., 2005).

According to Eq. 2, the FCO_2 variability depends mainly on the distribution of SST_{RS} and chl a_{RS} (used to estimate ΔfCO_2) and on the WS variability that controls the transfer velocity. The remaining monthly residuals of these variables significantly explained a total of 69% of the variance of FCO_2 at long-term trend exceeding the 95% confidence level. The transfer velocity was specifically the most influential variable explaining 57% of the long-term FCO_2 variability. As it was previously described, the WS dataset obtained from NCEP/NCAR Reanalysis project showed no clear year-to-year trend. However, WS events of high intensity were really observed a long-term reduction of -0.6±0.3 $m \cdot s^{-1} \cdot yr^{-1}$ that was statistically significant at the 89% throughout the study period while the lowest WS periods showed no-trend. Therefore the seasonal WS variability also loses amplitude at a rate of -0.6±0.3 $m \cdot s^{-1} \cdot yr^{-1}$ (p-value<0.17) from 1998 to 2004. Then, the transfer velocity in spite of not showing any long-trend variability is mainly slowing down during months of higher WS (Table 1; Fig. 6c) that also correspond to those of stronger ΔfCO_2 affecting considerably the net CO_2 uptake from the atmosphere. Additionally, the no-seasonal variability of SST_{RS} and chl a_{RS} slightly explain the FCO_2 reduction representing 10% and 2%, respectively.

4. Conclusions

The empirical algorithm described by Ono et al. (2004) was successfully used for predicting the fCO_2^{sw} measurements of the Bay of Biscay from remotely sensed SST and chl *a*. The computational approach fits adequately in situ fCO_2^{sw} measurements reporting a regression error of 0.1±7.5 µatm. The maximum differences were found during the last stage of the spring bloom in which the fingerprint of the biological uptake in the low fCO_2^{sw} levels remain after the disappearance of the phytoplankton community by grazing or settling.

The FCO_2 estimations extended from September 1997 to December 2004 showing a mean value of -2.5±0.3 $mol \cdot m^{-2} \cdot yr^{-1}$ and characterizing the Bay of Biscay as a predominant sink of atmospheric CO_2. This CO_2 uptake shows an appreciable reduction at a rate of 0.08±0.05 $mol \cdot m^{-2} \cdot yr^{-2}$ that was explained in 57% by the transfer velocity variability pointing out the wind speed as the key parameter controlling the long-term FCO_2 variability. The cooling of surface waters of the Bay of Biscay at a rate of ~ 0.06±0.03ºC·yr^{-1} explained 10% of the weakening of CO_2 sink strength whereas 2% was explained by the long-term variability of the chlorophyll concentration.

5. Acknowledgments

This work was developed and funded by the ECO project (MCyT REN2002-00503/MAR) and by the European Commission project (EU FP6 CARBOOCEAN Integrated Project, Contract no: 511176-2). “Diputación de Pontevedra” financed X.A. Padin with a predoctoral grant. We want to thank especially the Captains and crew of *RO-RO L’Audace* and *RO-RO Surprise*, and the management team from Suardiaz Company, for their hospitality and essential help throughout the two years. The authors also wish to thank the distributors of WOD01 salinity data (http://www.nodc.noaa.gov/), the SeaWiFS images (http://daac.gsfc.nasa.gov/), the SST images (http://podaac.gsfc.nasa.gov/). Wind and sea level pressure data were provided by NCEP Reanalysis (NOAA-CIRES Climate Diagnostics Center, Boulder, Colorado,

USA, from their Web site at http://www.cdc.noaa.gov/). We would also like to thank the NOAA/ESRL Global Monitoring Division for providing the atmospheric CO_2 flask data. Satellite images have been processed in Remote Sensing Service at ICMAN-CSIC.

References

Beaufort, L. and Heussner, S., 1999. Coccolithophorids on the continental slope of the Bay of Biscay – production, transport and contribution to mass fluxes. Deep Sea Research II, 46:2147– 2174.

Borges, A.V., Delille, B., Frankignoulle, M., 2005. Budgeting sinks and sources of CO_2 in the coastal ocean: Diversity of ecosystems counts. Geophysical Research Letters, 32, L14601, doi:10.1029/2005GL023053.

Brown, C.W. and Yoder, J.A., 1994. Coccolithophorid blooms in the global ocean. Journal of Geophysical Research, 99:7467–7482.

Campbell, J.W., Blaisdell, J.M., Darzi, M., 1995. Level-3 SeaWiFS data products: spatial and temporal binning algorithms. In: Hooker, S. B.; Firestone, E. R. ed. NASA Technical Memorandum 104566 (SeaWiFS Technical Report Series), vol. 32. 69p.

Cooper, D.J., Watson, A.J. and Ling, R.D., 1998. Variation of pCO_2 along a North Atlantic shipping route (U.K. to Caribbean): A year of automated observations. Marine Chemistry, 60:147–164.

Corbière, A., N. Metzl, G. Reverdin, C. Brunet, Takahashi, T., 2007. Interannual and decadal variability of the carbon dioxide sink in the North Atlantic subpolar gyre, Tellus, Ser. B, 59, 168–178.

DOE, 1994. Handbook of methods for the analysis of the various parameters of the carbon dioxide system in sea water, version 2. ORNL/CDIAC-74.

Goes, J.I., Saino, T., Oaku, H., Ishizaka, J., Wong, C.S. and Nojiri, Y., 2000. Basin scale estimates of sea surface nitrate and new production from remotely sensed sea surface temperature and chlorophyll. Geophysical Research Letters, 27:1263–1266.

Goyet, C., Millero, F.J., O'Sullivan, D.W., Eischeid, G., McCue, S.J. and Bellerby, R.G.J., 1998. Temporal variations of pCO_2 in surface seawater of the Arabian Sea in 1995. Deep Sea Research I, 45:609–623.

Gregg, W.W., Casey, N.W., McClain, C.R., 2005. Recent trends in global chlorophyll. Geophysical Research Letters, 32, L03606, doi:10.1029/2004GL021808.

Harlay, J., De Bodt, C., D'Hoop, Q., Borges, A.V., Suykens, K., Van Oostende, N., Sabbe, K., Roevros, N., Groom, S. and Chou, L. 2006. Biogeochemistry of a late marginal coccolithophorid bloom in the Bay of Biscay. Geophysical Research Abstracts, 9, 00710.

Hood, E.M., Merlivat, L. and Johannesse, T., 1999. fCO_2 variations and air-sea flux of CO_2 in the Greenland Sea gyre using high frequency time-series from the CARIOCA drift-buoys. Journal of Geophysical Research, 104:20571–20583.

Kilpatrick, K.A., Podestá, G.P., and Evans, R., 2001. Overview of the NOAA/NASA advanced very high resolution Pathfinder algorithm for sea surface temperature and associated database Journal of Geophysical Research, 106:9179–9197.

Körtzinger, A., Thomas, H., Schneider, B., Gronau, N., Mintrop, L., and Duinker, J.C., 1996. At sea intercomparision of two newly designed underway pCO2 systems-encouraging results. Marine Chemistry, 52:133–145.

Koutsikopoulos, C. and Le Cann, B., 1996. Physical processes and hydrological structures related to the Bay of Biscay anchovy. Scientia Marina, 60(2):9–19.

Lampert, L., Quéguiner, B., Labasque, T., Pichon, A., and Lebreton, N. 2002. Spatial variability of phytoplankton composition and biomass on the eastern continental shelf of the Bay of Biscay (north-east Atlantic Ocean). Evidence for a bloom of Emiliania huxleyi (Prymnesiophyceae) in spring 1998. Continental Shelf Research, 22:1225–1247.

Lee, K., Wanninkhof, R., Takahashi, T., Doney, S.C., and Feely, R.A., 1998. Low interannual variability in recent oceanic uptake of atmospheric carbon dioxide. Nature 396:155–159.

Lee, K., Wanninkhof, R., Feely, R.A., Millero, F.J. and Peng, T.–H., 2000. Global relationship of total inorganic carbon with temperature and nitrate in surface seawater. Global Biogeochemical. Cycles, 14:979–994.

Lefevre, N. and Taylor, A., 2002. Estimating pCO_2 from sea surface temperatures in the Atlantic Gyres. Deep Sea Research I, 49:539–554.

Lefevre, N., Watson, A.J., Olsen, A., Ríos, A.F., Pérez, F.F. and Johannessen, T., 2004. A decrease in the sink for atmospheric CO_2 in the North Atlantic. Geophysical Research Letters, 31, L07306, doi:10.1029/2003GL018957.

Longhurst, A., 1998. Ecological geography of the sea. Academic Press, New York.

Metzl, N., Poisson, A., Louanchi, F., Brunet, C., Schauer, B. and Bres, B., 1995. Spatio-temporal distributions of air-sea fluxes of CO2 in the Indian and Antarctic oceans. Tellus, 47B:56–69.

Millero, F., Lee, K. and Rooche, M., 1998. Distribution of alkalinity in the surface ocean of the major oceans. Marine Chemistry, 60:111–130.

Nelson, N.B., Bates, N.R., Siegel, D.A. and Michaels, A.F., 2001. Spatial variability of the CO_2 sink in the Sargasso Sea. Deep Sea Research II, 48:1801–1821.

Olsen, A., Bellerby, R.G.J., Johannessen, J., Omar, A.M. and Skjelvan, I., 2003. Interannual variability in the wintertime air-sea flux of carbon dioxide in the northern North Atlantic. Deep Sea Research I, 50:1323–1338.

Olsen, A., Triñanes, J.A. and Wanninkhof, R., 2004. Sea–air flux of CO_2 in the Caribbean Sea estimated using in situ and remote sensing data. Remote Sensing of Environment, 89(3):309–325.

Omar, A. M., and A. Olsen (2006), Reconstructing the time history of the air-sea CO2 disequilibrium and its rate of change in the eastern subsolar North Atlantic, 1972–1989, Geophysical Research Letter, 33, L04602, doi:10.1029/2005GL025425.

Ono, T., Saino, T., Kurita, N. and Sasaki, K., 2004. Basin-scale extrapolation of shipboard pCO_2 data by using satellite SST and Chl a. International Journal of Remote Sensing, 25(19):3803–3815.

O'Reilly, J.E., Maritorena, S., Mitchell, G., Siegel, D.A., Carder, K.L., Garver, S.A., Kahru, M. and McClain, C.R., 1998. Ocean colour algorithms for SeaWiFS. Journal of Geophysical Research, 103:24937–24953.

Padin, X.A., Vázquez-Rodríguez, M., Ríos, A.F. and Pérez, F.F., 2007. Atmospheric CO_2 measurements and error analysis on seasonal air-sea CO_2 fluxes in the Bay of Biscay. Journal of Marine Systems, 66:285–296.

Paillet, J. and Mercier, H., 1997. An inverse model of the eastern North Atlantic general circulation and thermocline ventilation. Deep-Sea Research II, 44:1293–1328.

Patra, K.P., Maksyutov, S., Ishizawa, M., 2005. Interannual and decadal changes in the sea-air CO2 flux from atmospheric CO2 inverse modelling. Global Biogeochemical Cycles, 19, GV4013, doi: 10.1029/2004GV002257.

Planque, B., Beillois, P., Jégou, A.-M., Lazure, P., Petitgas, P. and Puillat, I., 2003. Large scale hydroclimatic variability in the Bay of Biscay. The 1990s in the context of interdecadal changes. ICES Marine Science Symposia, 219:61–70.

Raitsos, D.E., Lavender, S.J., Pradhan, Y., Tyrrel, T., Reid, P.C. and Edwards, M., 2006. Coccolithophore bloom size variation in response to the regional environment of the subartic North Atlantic. Limnology and Oceanography, 51(5):2122–2130.

Robertson, J.E. and Watson, A.J., 1993. Thermal skin effect of the surface ocean and its implications for CO_2 uptake. Nature, 358:738–740.

Robertson, J.E., Robinson, C., Turner, D.R., Holligan, P., Watson, A.J., Boyd, P., Fernandez, E. and Finch, M. 1994. The impact of a coccolithophore bloom on oceanic carbon uptake in the northeast Atlantic during summer 1991. Deep-Sea Research I, 41(2):297–314.

Sabine, C.L., Feely, R.A., Gruber, N., Key, R.M., Lee, K., Bullister, J.L., Wanninkhof, R., Wong, C.S., Wallace, D.W.R., Tilbrook, B., Millero, F.J., Peng, T.-H., Kozyr, A.,

Ono, T., and Ríos, A.F., 2004. The oceanic sink for anthropogenic CO2. Science, 305: 367–371.

Sarmiento, J.L. and Le Queré, C., 1996. Oceanic carbon dioxide uptake in a model of century-scale global warming. Science, 274:1346–1350.

Schuster, U. and Watson, A.J., 2007. A variable and decreasing sink for atmospheric CO2 in the North Atlantic. Journal of Geophysical Research, 112, C11006, doi:10.1029/2006JC003941.

Stephens, M.P., Samuels, G., Olson, D.B., Fine, R.A. and Takahashi, T., 1995. Sea-air flux of CO_2 in the North Pacific using shipboard and satellite data. Journal of Geophysical Research, 100:13571–13583.

Takahashi, T., 1961. Carbon dioxide in the atmosphere and in Atlantic ocean water. Journal of Geophysical Research, 66:477–494.

Takahashi, T., Olafsson, J., Goddard, J.G., Chipman, D.W. and Sutherland, S.C., 1993. Seasonal variation of CO_2 and nutrients in the high latitude surface oceans: A comparative study. Global Biogeochemical Cycles, 7:843–878.

Takahashi, T. 2002. Global air-sea flux of CO_2: an estimate based on measurements of sea-air pCO_2 difference. Lammont-Doherty Earth Observatory of Columbia University website http://ingrid.ldgo.columbia.edu/SOURCES/LDEO/Takahashi/dataset_documentation.html.

Tans, P.P., Fung, I.Y. and Takahashi, T., 1990. Observational constraints on the global atmospheric CO_2 budget. Science, 247:1431–1438.

Tyrrell, T. and Taylor, A. H., 1995. Latitudinal and seasonal variations in carbon dioxide and oxygen in the northeast Atlantic and the effects on Emiliania huxleyi and other phytoplankton. Global Biogeochemical Cycles, 9:585–604.

Wanninkhof, R., 1992. Relationship between wind speed and gas exchange over the ocean. Journal of Geophysical Research, 97:7373-7382.

Weiss, R. F. 1974. Carbon dioxide in water and seawater: The solubility of a nonideal gas. Marine Chemical, 2:201–215.

Figure captions

Figure 1: The Bay of Biscay showing the regular ECO route (black line) between Vigo (Spain) and St. Nazaire (France) and the inner part of the Bay of Biscay (grey frame) with the locations of the discrete samples of chlorophyll (white circles).

Figure 2: Differences and box plot of residuals between (a) sea surface temperatures retrieved by AVHRR and shipboard measurements and between (b) chlorophyll concentrations obtained from SeaWiFS sensor and shipboard measurements. Residuals between (c) the fCO_2 computed and the observed fCO_2 throughout the year 2003. Dates of cruises (black vertical lines) and of chlorophyll sampling (black circle) are marked on top of the Figure.

Figure 3: Scatter plots of fCO_2^{sw} against chl a_{RS}. Gray dots correspond to the shipboard data and white dots correspond to the data computed from the empirical algorithm.

Figure 4: Climatological maps of ΔfCO_2 and FCO_2 for January, April, July and October.

Figure 5: Monthly means (white circles) and standard deviations (error bars) of SST_{RS} (a), chl a_{RS} (b), ΔfCO_2 (c), wind speed (d) and FCO_2 (e) of the inner part of the Bay of Biscay from September 1997 to December 2004.

Figure 6: Long-term trend with the respective errors at a seasonal scale and of SST_{RS} (a), chl a_{RS} (b), ΔfCO_2 (c), WS (d) and FCO_2 (e).

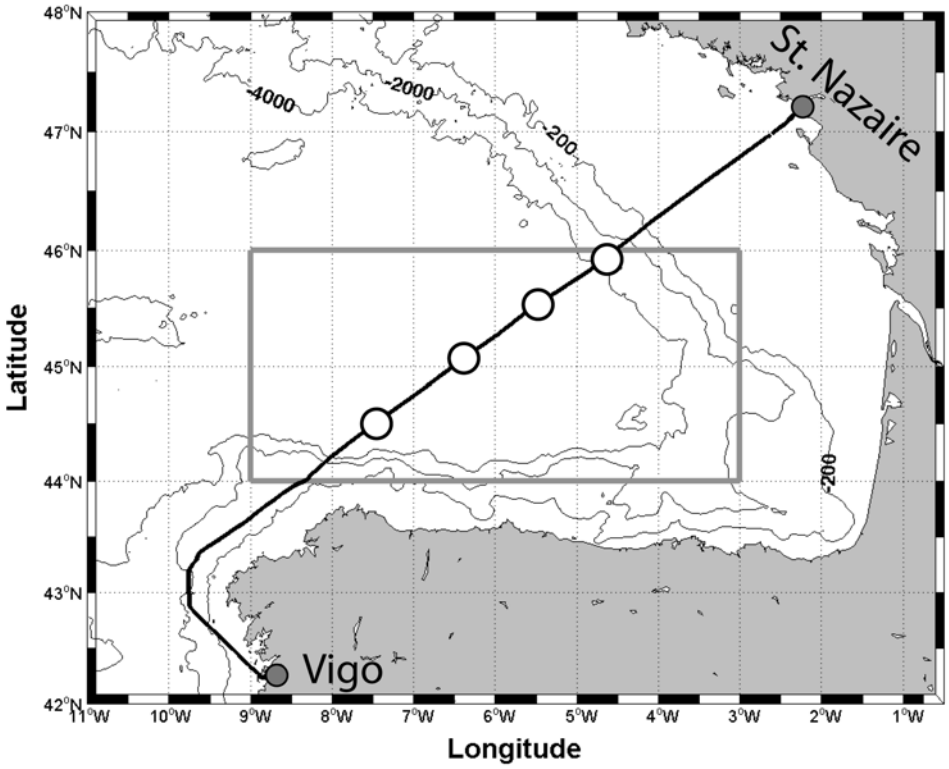

Figure 1

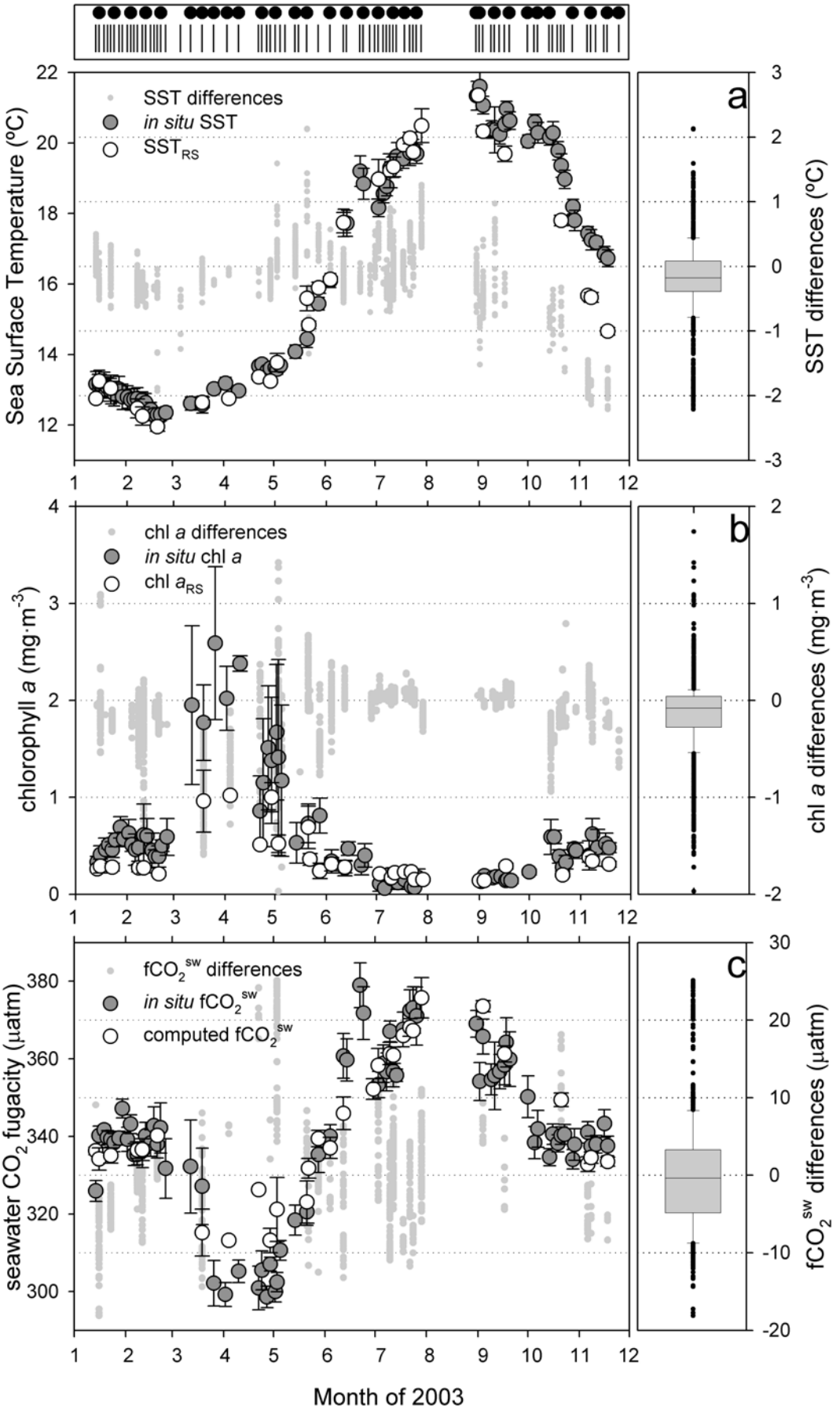
SST differences
in situ SST
SST$_{RS}$
Sea Surface Temperature (ºC)
SST differences (ºC)
a
chl a differences
in situ chl a
chl a$_{RS}$
chlorophyll a (mg·m^{-3})
chl a differences (mg·m^{-3})
b
fCO$_2^{sw}$ differences
in situ fCO$_2^{sw}$
computed fCO$_2^{sw}$
seawater CO$_2$ fugacity (µatm)
fCO$_2^{sw}$ differences (µatm)
c
Month of 2003

1

Figure 2

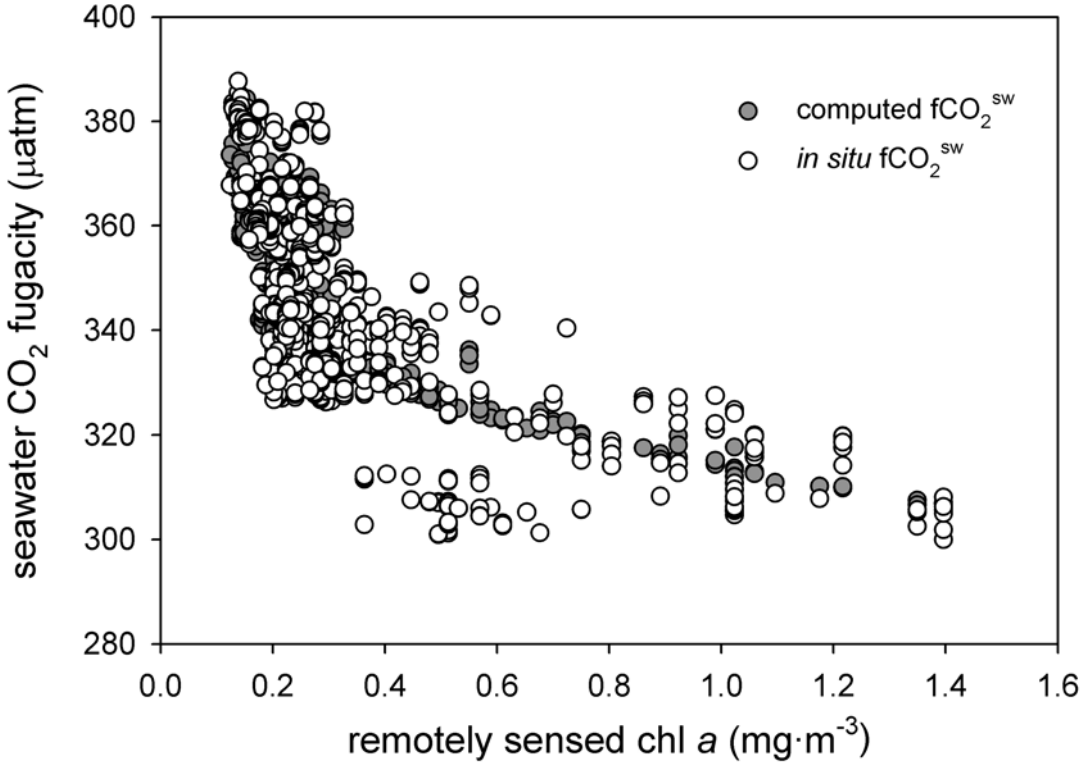

Figure 3

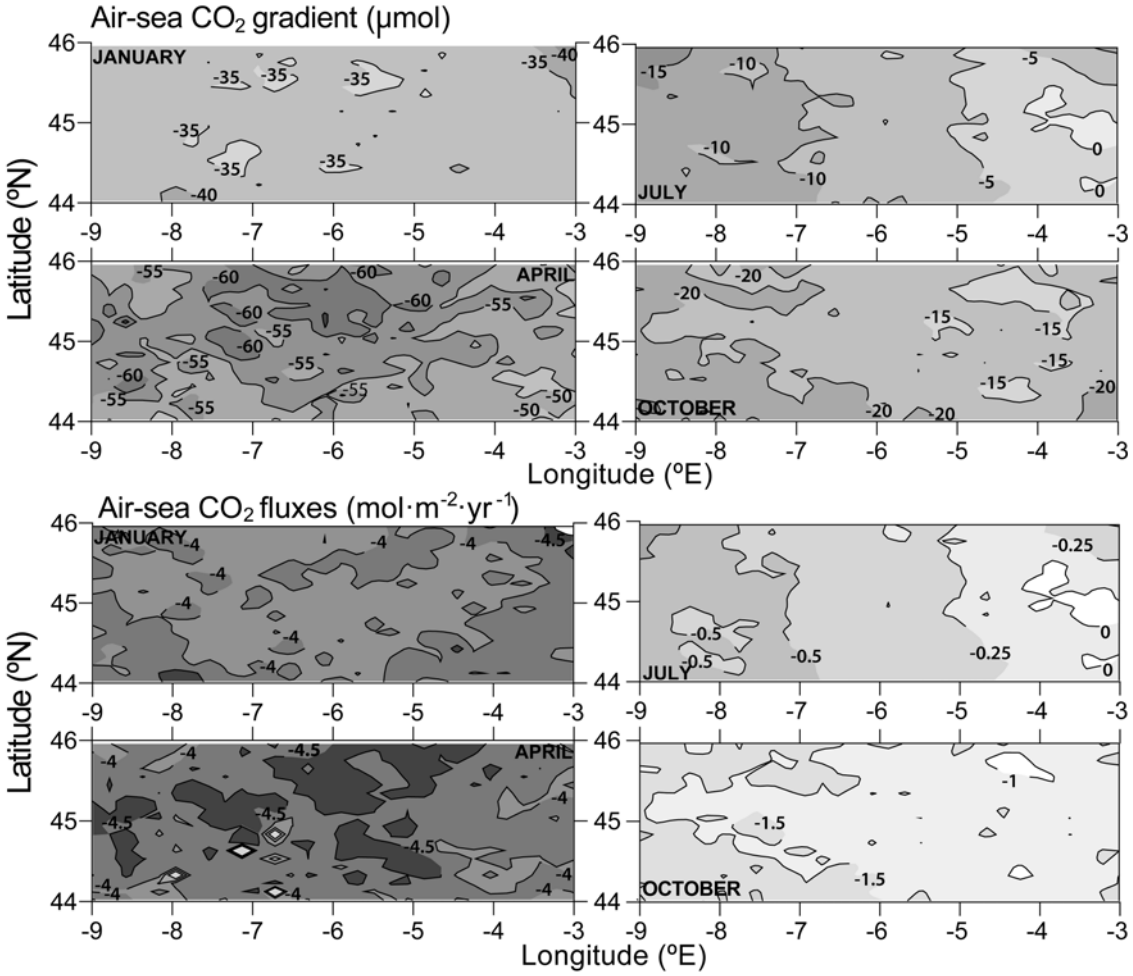
Air-sea CO_2 gradient (µmol)
JANUARY
JULY
APRIL
OCTOBER
Latitude (ºN)
Longitude (ºE)
Air-sea CO_2 fluxes (mol·m^{-2}·yr^{-1})
JANUARY
JULY
APRIL
OCTOBER
Latitude (ºN)
Longitude (ºE)

Figure 4

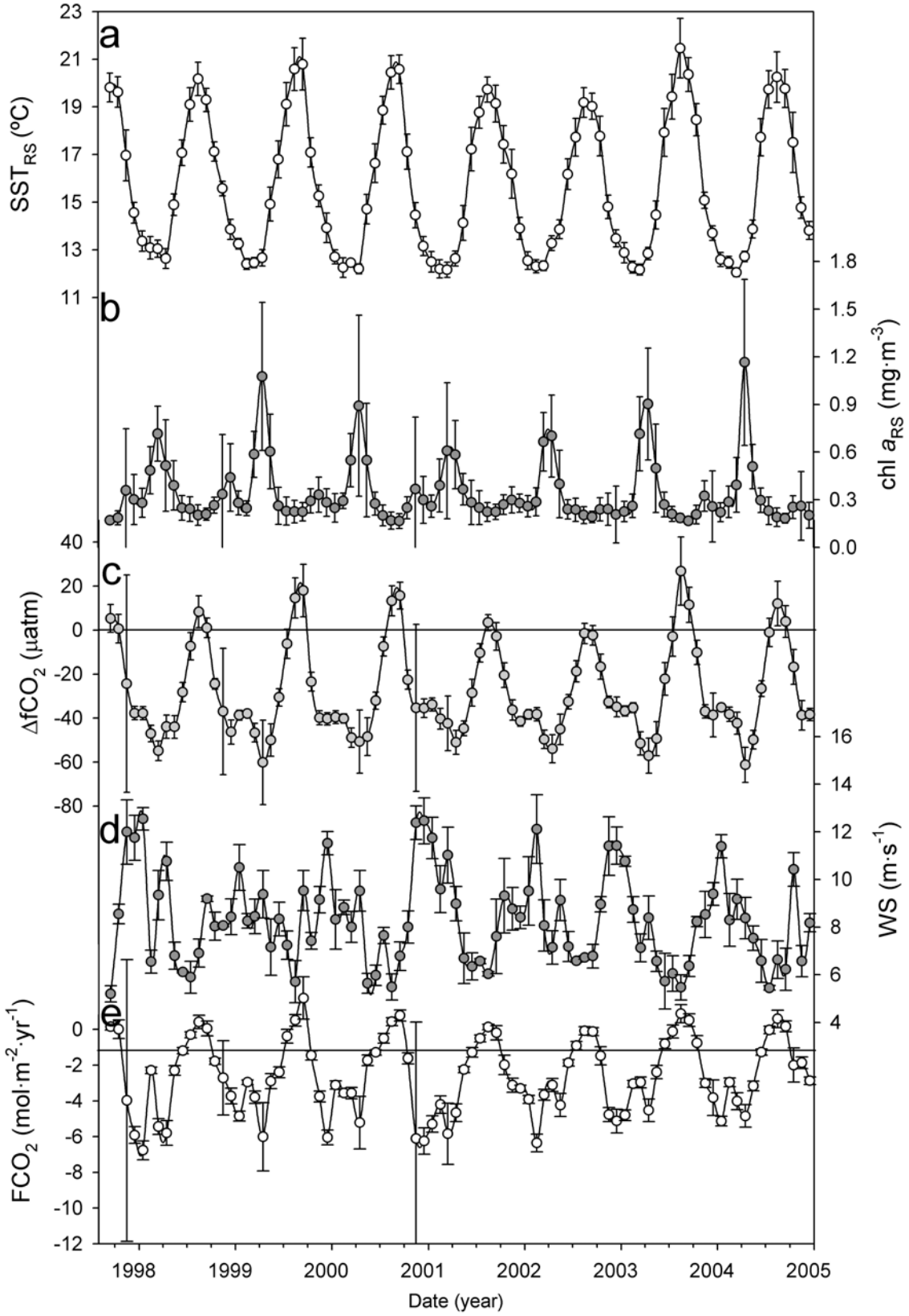
a
b
c
d
e
SST$_{RS}$ (ºC)
chl a_{RS} (mg·m^{-3})
ΔfCO$_2$ (µatm)
WS (m·s^{-1})
FCO$_2$ (mol·m^{-2}·yr^{-1})
Date (year)
1998
1999
2000
2001
2002
2003
2004
2005

Figure 5

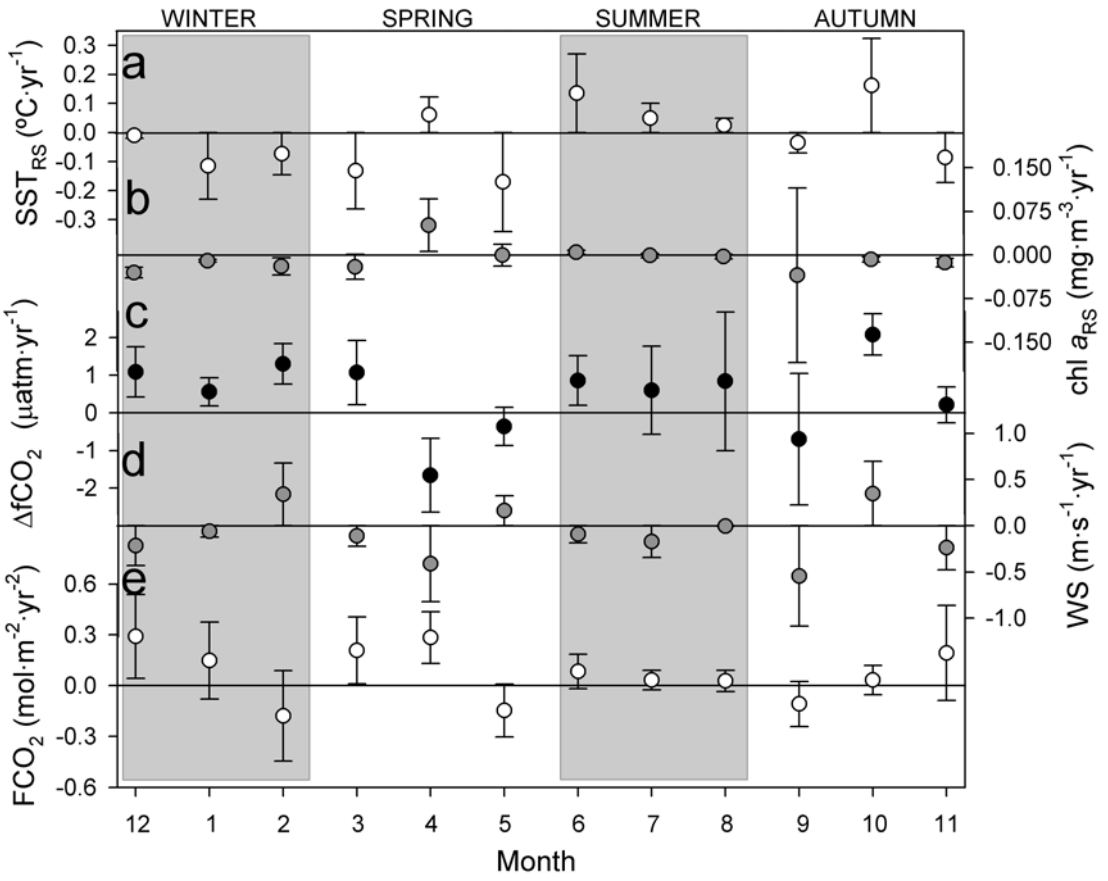

Figure 6

Table 1: Means and standards deviations for each month between September 1997 and December 2004 of air-sea fCO_2 gradient (ΔfCO_2), remote sensing temperature (SST_{RS}), chlorophyll ($Chla_{RS}$) and wind speed (WS) and air-sea CO_2 exchange (FCO_2).

	ΔfCO_2 (μatm)	SST_{RS} (ºC)	$Chla_{RS}$ ($mg \cdot m^{-3}$)	WS ($m \cdot s^{-1}$)	FCO_2 ($mol \cdot m^{-2} \cdot yr^{-1}$)
January	-37±4	12.8±2.8	0.25±0.02	9.2±1.2	-4.0±1.0
February	-39±4	12.4±2.5	0.32±0.09	7.9±1.3	-2.8±0.9
March	-48±5	12.4±2.1	0.60±0.11	7.9±0.9	-3.4±0.8
April	-55±6	12.7±3.4	0.83±0.24	8.2±1.5	-4.0±1.0
May	-48±5	14.4±1.9	0.47±0.09	6.5±1.0	-2.3±0.7
June	-29±4	17.1±1.4	0.27±0.02	5.9±1.0	-1.2±0.5
July	-8±6	19.0±0.6	0.23±0.02	5.9±0.4	-0.3±0.2
August	11±9	20.3±0.7	0.20±0.02	5.6±0.6	0.3±0.3
September	6±9	19.8±1.5	0.19±0.02	6.7±1.2	0.3±0.6
October	-17±5	17.8±0.9	0.25±0.03	8.0±0.8	-1.3±0.3
November	-35±2	15.4±2.7	0.31±0.04	8.5±1.5	-3.0±1.0
December	-39±4	13.8±1.7	0.28±0.08	8.9±0.8	-3.4±0.6